Int. J. Solids Structures Vol. 29, No. 11, pp. 1417–1431, 1992
Printed in Great Britain.

0020-7683/92 $5.00 + .00

AN ECCENTRIC SHEAR-LAG MODEL AND IMPLICATIONS ON THE STRENGTH OF FIBROUS COMPOSITES

Y. WEITSMAN and A. I. BELTZER†
Department of Engineering Science and Mechanics, The University of Tennessee, 310 Perkins Hall, Knoxville, TN 37996, U.S.A.

(*Received* 19 *November* 1990; *in revised form* 17 *September* 1991)

Abstract—The stress field in the vicinity of a broken fiber-reinforced composite is analysed by means of a shear-lag model. The broken filament is positioned eccentrically relative to its neighboring fibers to simulate the commonplace non-uniformity of fiber spacing within the transverse plane. It is shown that a fiber break gives rise to severe bending, in addition to tension, in the neighboring fibers—with a substantial overstress focused on the nearest unbroken filament. The complex nature of the stress field, which is caused by the failure of a fiber within a composite casts doubt on the applicability of failure statistics derived from tensile failure data of single fibers, which is commonly used to predict the strength of composites.

1. INTRODUCTION

Concentric shear-lag models have been used extensively in the analysis of composites, in particular, in the context of micromechanical aspects of failure [see, for example, Hull (1981)]. Indeed, the interplay between micromechanics and the statistics of fiber failure appears to be the most difficult aspect in modeling the strength of fibrous composites.

Due to the complexity of the phenomenon, the theoretical analyses invoke a variety of assumptions, the influence of which may be difficult to assess. One of the basic approaches was set forth by Gücer and Gurland (1962) who represented a material as a series of layers. Each layer was considered to consist of fiber-like elements loaded in parallel, which allows for the use of the bundle theory (Daniels, 1945) to analyse its strength. The overall failure of the layered structure may then be predicted by the weakest link approach. This theory has left, however, the layer thickness unspecified. Rosen (1965), proposed to identify this parameter as the so-called fiber ineffective length, δ, and provided a definition of this quantity.

Since then this approach, which combined micromechanical and statistical considerations, has been of particular interest in failure investigations. Garg *et al.* (1973), provided a good exposition of the approach, which has remained of particular interest up to the present time, such as in the recent investigations of composite failure by Prewo (1986) and Schwietert and Steif (1990).

As noted earlier, the models of statistical strength are essentially approximate and invoke various assumptions. A fortuitous agreement with experiments may, therefore, well occur. It is instructive that a prediction of failure which is based upon the simple-minded rule of mixtures appears to fit the experiments reported by Prewo (1986) fairly well, while a much more sophisticated approach by Zweben and Rosen (1970) provides good results only if the ineffective length is taken to be orders of magnitude larger than the value derived from the theoretical analysis. Thus, it becomes clear that there may be important micromechanical and other factors, which were overlooked by the analysis.

To discuss these factors we recall the basic result given by Rosen (1965) as follows

† Permanent address: Holon Institute of Technological Education. Affiliated with Tel-Aviv University, P.O. Box 305, Holon 58102, Israel.

$$\frac{\sigma_f^*}{\sigma_f} = \left(\frac{\delta}{L}\right)^{(\beta+1)/\beta} \Gamma(1+1/\beta). \tag{1}$$

Here σ_f^* and σ_f are the statistical mode of composite failure stress and the mean tensile strength of an individual fiber, respectively, δ and L are the ineffective length and the fiber length, respectively, β is a material constant which appears in the Weibull strength distribution, and $\Gamma(\cdot)$ is the Gamma function. One observes, from eqn (1), that the composite mechanical behavior manifests itself through the ineffective length δ, while the statistical nature of the phenomenon is introduced through the material constant, β, which is obtained from failure data for "dry" fibers in pure tension.

There appear to be two major arguments which cast doubt on the accuracy of eqn (1) and its underlying methodology. The first argument, forwarded by McCarthy and Orringer (1975), indicates that statistical strength data obtained for tensile loading of fibers involve samples with lengths of about 1 in. On the other hand, according to the analysis of Rosen (1965), the ineffective length, δ, which specifies the layer thickness in eqn (1), is usually between 10 and 40 microns. This brings into question the validity of the value of β, as obtained from fiber tensile tests, in predicting the strength of composites.

The second argument deals with the absence of load concentration effects in eqn (1). Zweben (1968) and Zweben and Rosen (1970), attempted to modify the theory in order to account for these effects. While the overload suffered by the fibers adjacent to a broken filament does indeed play an essential role in the failure mechanism, the above works still do not provide a satisfactory agreement with experiments (Prewo, 1986).

The above observations show that there may be factors which are overlooked by the previous analyses. Among these we would particularly note the randomness of the fiber location in the transverse plane. Typical micrographs, for graphite BMI and graphite/epoxy composites are shown in Figs 1(a, b), while results of Monte-Carlo simulations are exhibited in Figs 2(a, b). It is obvious that since fibers are not uniformly spaced within the cross-sections, the concentric shear-lag model does not account for this commonplace phenomenon within composites.

The eccentric model, introduced herein, reveals essential effects induced by the above mentioned randomness. The present investigation indicates that in contrast with the premises of bundle theory, the failure of a filament in a composite causes a complicated stress field in the vicinity of the break. Specifically, the neighboring fibers suffer extensive bending, in addition to tension, and may therefore be subjected to failure mechanisms other than those associated with pure tension. Though bending in neighboring fibers occurs even in concentric configurations around a broken filament, eccentricity serves to accentuate bending effects. It is shown in the present paper that, with rather commonplace eccentricities, the overload due to bending may be quite substantial, with values of about twice those of the intact case.

Consequently, the present micromechanical analysis casts further doubt on the applicability of the commonly used statistical data obtained for free fibers in pure tension to the prediction of strength of fibrous composites.

2. ANALYSIS

Shear-lag models, which abound in the mechanics literature, provide useful approximations for the mechanism of force transfer between "soft" and "hard" material components such as layered structures or fiber reinforced composite materials. The formulation of all these models derives from the common assumption that the "soft" material responds only in shear, while the "hard" matter alone carries the entire normal load.

When applied to load transfer mechanisms in uniaxially reinforced polymeric composites this assumption appears to provide an excellent approximation in many important circumstances. For instance, under tension parallel to the fiber direction, the fibers carry 95–99% of the applied load. It can also be shown that their shear distortion amounts to no more than 5% of their normal strain.

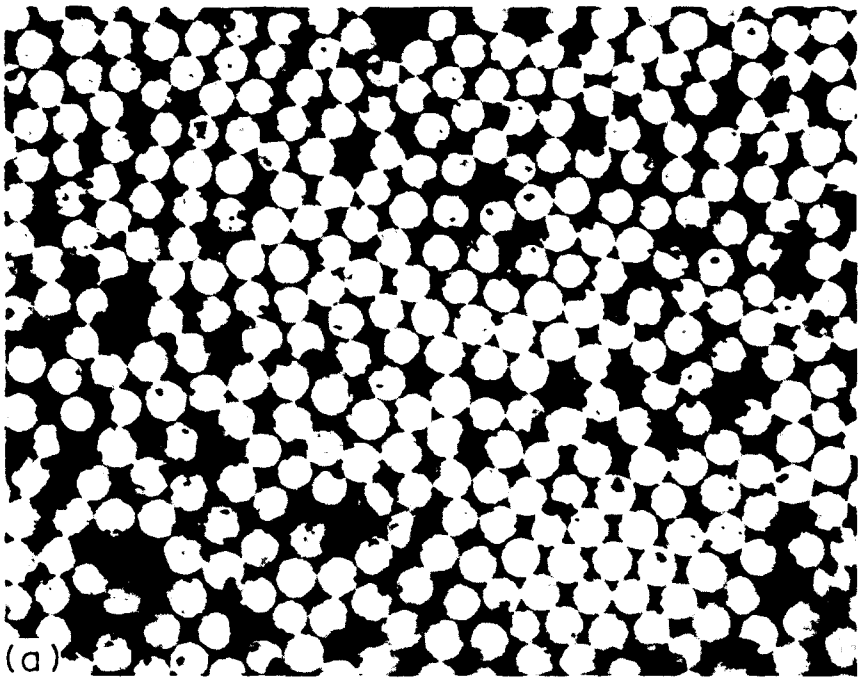

Fig. 1a. A typical cross-section of graphite BMI composite, estimated volume fraction $v_f = 55\%$ (courtesy of Professor W. W. Stinchcomb) (× 1000).

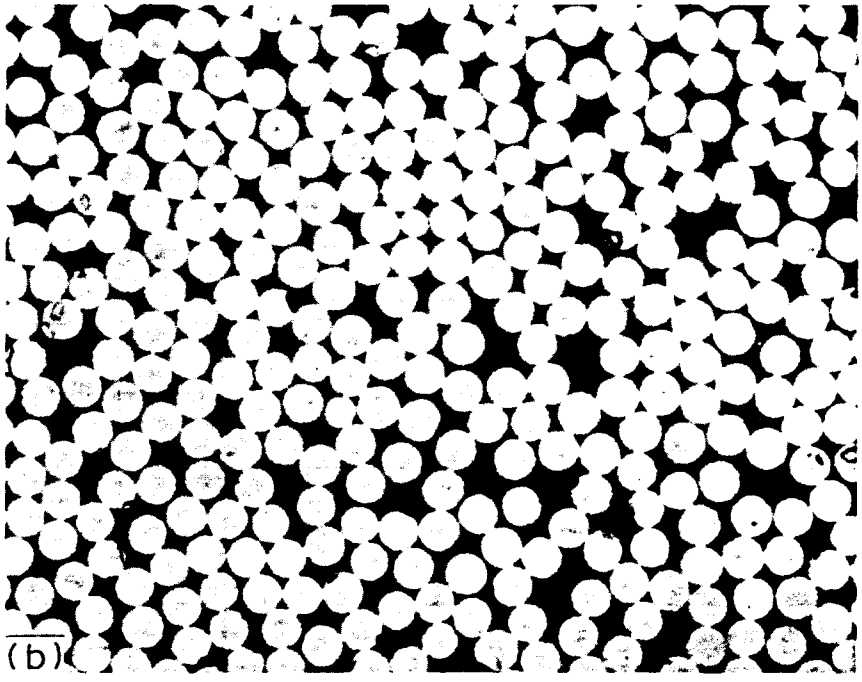

Fig. 1b. A typical cross-section of graphite/epoxy composite, estimated volume fraction $v_f = 65\%$ (courtesy of Professor W. W. Stinchcomb) (× 1000).

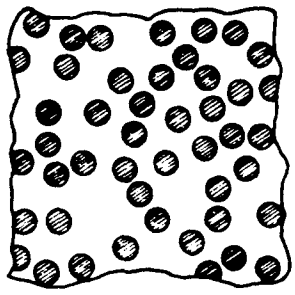

Fig. 2a. Monte-Carlo simulation of a cross-section with fiber volume fraction $v_f = 40\%$.

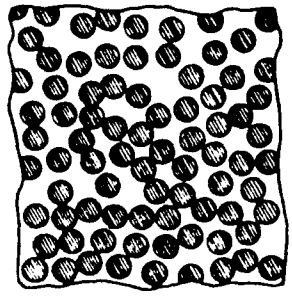

Fig. 2b. Monte-Carlo simulation of a cross-section with fiber volume fraction $v_f = 65\%$.

Since our analysis of the eccentric case is constructed as a perturbation from the concentric configuration, it is helpful to formulate the concentric case in a form which is readily amenable to the perturbation scheme.

2.1. *A shear-lag model for the concentric case*

Consider the central fiber, f, of radius a positioned within a perfect hexagonal array of neighboring fibers. Also, let h denote the distance between the centers of adjacent fibers and b the outer radius of the "shear zone" as shown in Figs 3a, b.†

The fiber volume fraction is given by $V_f = 2\pi a^2/\sqrt{3}h^2$ whereby

$$h = \sqrt{2\pi/(\sqrt{3}V_f)}a \quad \text{and} \quad b = h - a = (\sqrt{2\pi/(\sqrt{3}V_f)} - 1)a.$$

Let r, θ, z denote cylindrical coordinates and consider a uniaxially reinforced composite of infinite extent which consists of a perfect, hexagonal fibrous array, subjected to uniform axial stress $\sigma_z = \sigma_a$ at $|z| \to \infty$.

In view of the foregoing arguments we neglect the tensile load carried by the matrix and assume that the applied stress is carried entirely by the fibers, with $\sigma_z^f = \sigma_a/V_f$ denoted by $\sigma_z^f = \sigma_0$. This approximation is equivalent to neglecting the ratio $E_m V_m/E_f V_f$ which, for polymeric composites, is $0(10^{-2})$.

Consider now the case of a single broken fiber at $z = 0$. The effect of this break can be analysed by superposition of the "undisturbed" solution $\sigma_z^f = \sigma_0$ and the solution to the disturbance caused by $\sigma_z^f(r, \theta, 0) = -\sigma_0$ $(0 \leqslant r \leqslant a, 0 \leqslant \theta < 2\pi)$.

In accordance with the shear lag assumption, we shall account for the above mentioned "disturbance" by means of normal stress $\sigma_z^f(r, \theta, z)$ in the fiber and a shear stress $\tau_{rz}^m(r, \theta, z)$ in the surrounding matrix. Specifically, the solution will be based upon the following assumptions:

(a) the only non-vanishing displacement is $u_z = u_z(r, z)$;

† Note that since $(a/b)^2 \neq v_f$ the "shear layer" $a < r < b$ extends *beyond* the representative volume element which is used in analyses of effective properties. Therefore the two cylinders with radii a and b should not be confused with the concentric cylinders employed in the "three phase model" (Christensen, 1979).

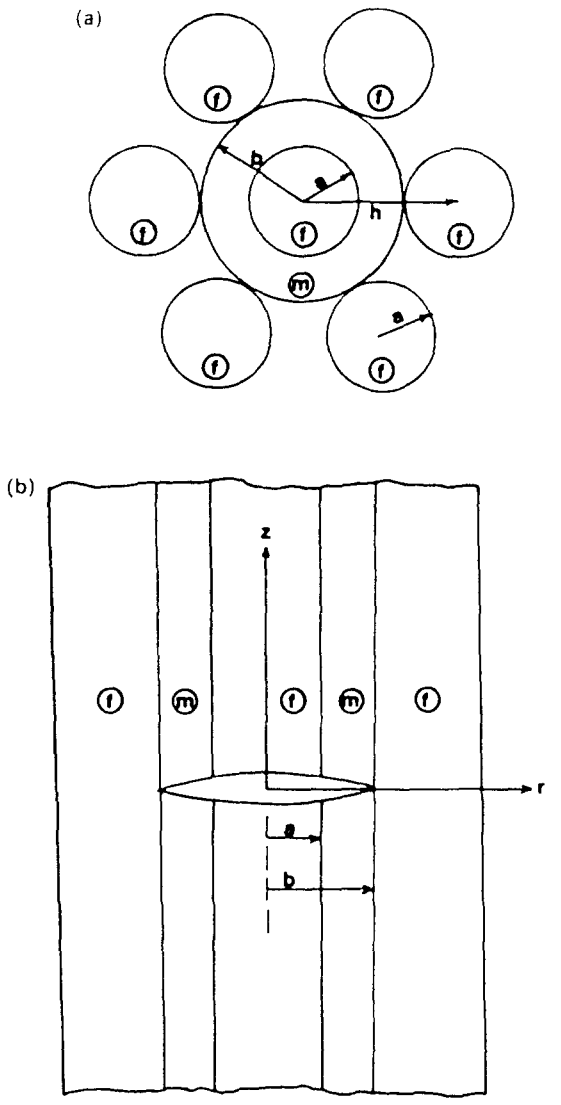

Fig. 3. A perfect hexagonal fibrous array, with broken central fiber f, surrounded by a concentric "sleeve" m of matrix material in shear. (a) Cross-sectional view. (b) Side view.

(b) discard the shear deformation in the broken fiber, whereby

$$u_z^f = f(z), \quad 0 \leqslant r < a, \quad 0 \leqslant z < \infty \tag{2}$$

and

$$\sigma_z^f = E_f f'(z); \tag{3}$$

(c) discard the contribution of normal stresses to the response of the matrix. Consequently, in the region $a < r < b$ consider only the shear strain $\gamma_{rz}^m = \partial u_z^m/\partial r$, shear stress $\tau_{rz}^m = G_m \gamma_{rz}^m$ as well as equilibrium governed by

$$\frac{\partial \tau_{rz}^m}{\partial r} + \frac{\tau_{rz}^m}{r} = 0. \tag{4}$$

The ostensible inconsistency of having $\tau_{rz}^f(a) \neq \tau_{rz}^m(a)$ can be explained by the same rationale employed in the Bernoulli–Euler beam theory, namely, the shear

stresses that act upon the broken fiber can be determined as a reaction, rather than from constitutive relations;

(d) the displacement u_z^m vanishes at $r = b$.

In addition, the shear-lag model enables the satisfaction of the displacement continuity condition at $r = a$ and "global" equilibrium for the broken fiber.

In view of the foregoing assumptions we construct the solution to the present problem as follows:

By the hypothesis $u_z^f = f(z)$, consequently consider $u_z^m = f(z)g(r)$ $(a \leqslant r \leqslant b, 0 \leqslant z < \infty)$.

From the equilibrium condition (4) we get $g'' + g'/r = 0$, hence $g(r) = A + B \ln r$. The conditions $u_z^m(z, a) = u_z^f(z, a)$ and $u_z^m(z, b) = 0$ yield

$$u_z^m = \frac{\ln (b/r)}{\ln (b/a)} f(z). \tag{5}$$

Finally, force equilibrium in the z-direction for the fiber gives

$$\pi a^2 \frac{\mathrm{d}\sigma_z^f}{\mathrm{d}z} + 2\pi a \tau_{rz}^m(a, z) = 0 \tag{6}$$

which, upon employment of eqns (3) and (5), gives

$$f''(z) - \frac{k^2}{a^2} f(z) = 0 \tag{7}$$

where

$$k^2 = \frac{2G_m}{E_f \ln (b/a)}.$$

Finally, the boundary conditions $\sigma_z^f = -\sigma_0$ at $z = 0$ and $\sigma_z^f = 0$ as $z \to \infty$ yield

$$f(z) = \frac{\sigma_0}{E_f} \frac{a}{k} \mathrm{e}^{-k(z/a)} \tag{8}$$

and $\sigma_z^f = -\sigma_0 \mathrm{e}^{-k(z/a)}$.

By superposition, the total stress on the broken fiber is

$$\sigma_z^{f(\mathrm{Total})} = \sigma_0 [1 - \mathrm{e}^{-k(z/a)}]. \tag{9}$$

A major shortcoming of all shear-lag models is their omission of transverse effects, such as the radial displacement u_r, which may give rise to substantial transverse stresses (e.g. σ_r) especially in the vicinity of the fiber break. However, since the main purpose of the present work is to accentuate the effects of fiber eccentricity, we do not attempt to correct the inherent deficiency of shear-lag models. Instead, we choose to illustrate our point by a consistent use of the above model, taking advantage of its relative simplicity.

2.2. *Eccentric shear lag*

It is conjectured that a reasonable estimate of the effects of random fiber spacings, exhibited in Figs 1 and 2, can be obtained by analysing the idealized circumstance of a perfect hexagonal array containing an eccentric central fiber f which is shifted to the right

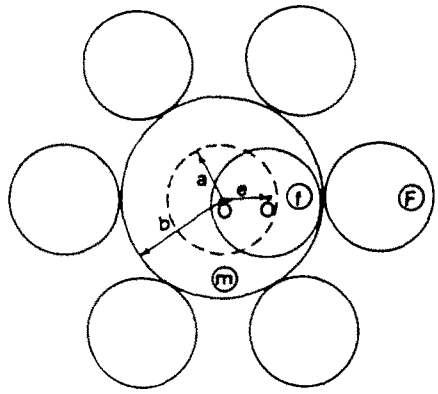

Fig. 4. A hexagonal fibrous array as in Fig. 3, with broken eccentric fiber f, eccentricity e and nearest neighboring fiber F.

by a distance e toward the nearest neighboring fiber F, as shown in Fig. 4. (The circle drawn in dashed lines shows the concentric position of that fiber.)

Consider now a cylindrical coordinate system r, θ, z centered at point O, instead of $\bar{O}$, but retain the boundary conditions $u_z^m = 0$ at $r = b$ on a cylindrical boundary which is centered about $\bar{O}$. This eccentric boundary value problem can be solved by means of a perturbation scheme which employs $\eta = e/b$ as a perturbation parameter. Such schemes were discussed by Van Dyke (1964) for cases which apply in fluid mechanics and modified by Parnes and Beltzer (1986) to circumstances appropriate for solids. In those schemes the perturbations occur in the shapes of the boundaries but not in the governing field equations, which remain linear.

In our computations we shall consider the circumstance of maximum eccentricity within the idealized configuration shown in Fig. 4 (when $e = b-a$, $\eta = (b-a)/b$), accounting for the effects of the commonplace randomness of the arrays shown in Figs 1 and 2.

Obviously, when the inner fiber breaks at $z = 0$ the eccentricity will give rise to non-uniform shear stresses τ_{rz}^m around the fiber-matrix interface. These stresses may vary not only along the z-direction, but also with the angle θ, and they attain their highest values at the place of nearest approach. Consequently, that fiber will be subject to bending moments and undergo rotations in addition to normal deformation.

In line with assumptions (a)–(d) of the previous section we now consider

$$u_z^f(r, \theta, z) = f(z) + \eta\beta(z) r \cos\theta \quad (0 \leqslant r \leqslant a, 0 \leqslant \theta < 2\pi, 0 \leqslant z \leqslant \infty). \tag{10}$$

Equation (10) implies that fiber deformation satisfies the hypothesis that "planes remain planes".

Within the matrix region $a \leqslant r \leqslant b$ the displacement u_z^m and the shear stress τ_{rz}^m depend on θ, and eqn (4) must be replaced by

$$\frac{\partial \tau_{rz}^m}{\partial r} + \frac{\tau_{rz}^m}{r} + \frac{1}{r}\frac{\partial \tau_{\theta z}^m}{\partial \theta} = 0 \tag{11}$$

with

$$\tau_{rz}^m = G_m \frac{\partial u_z^m}{\partial r} \quad \text{and} \quad \tau_{\theta z}^m = G_m \frac{1}{r}\frac{\partial u_z^m}{\partial \theta}. \tag{12}$$

Let $u_z^m(r, \theta, z) = q(z)p(r, \theta)$ then employment of (11) and (12) yields

$$\left(\frac{\partial^2}{\partial r^2}+\frac{1}{r}\frac{\partial}{\partial r}+\frac{1}{r^2}\frac{\partial^2}{\partial\theta^2}\right)u_z^m=0$$

whereby

$$u_z^m=p(z)\left\{A+B\ln r+\sum_{m=1}^{\infty}(A_m r^m+B_m r^{-m})\cos m\theta\right\} \tag{13}$$

where even symmetry in θ was considered without loss of generality.

Expressions (10) and (13) are readily amenable to a solution by the perturbation method of Parnes and Beltzer (1986), employing the eccentricity η as the perturbation parameter. Although this method can be carried to any desired degree of accuracy by expanding to ever higher powers of η, we deliberately refrain from going beyond the first power in η in deriving our estimate for the effects of fiber eccentricity. We eschew the employment of higher order expansions because the idealization involved in selecting the configuration shown in Fig. 4 to represent the behavior of random arrays, such as shown in Figs 1 and 2, leads us to believe that higher order mathematical accuracy may, in fact, be devoid of physical content. Nevertheless, an expansion to $0(\eta^3)$ is given in the Appendix to demonstrate the applicability of the perturbation technique.

Employment of the expression (10) and the form given in eqn (13), together with the requirement that $u_z^f(a,\theta,z)=u_z^m(a,\theta,z)$ and the assumption $u_z^m(b,\theta,z)=0$, in accordance with details given in the Appendix, yields

$$u_z^m(r,\theta,z)=\frac{f(z)}{\ln(b/a)}\left[\ln(b/r)+\eta\frac{a^2b/r-br}{b^2-a^2}\cos\theta\right]+\eta\beta(z)\frac{a^2}{b^2-a^2}\left(\frac{b^2}{r}-r\right)\cos\theta,$$

$$a\leqslant r\leqslant b,\quad 0\leqslant\theta<2\pi. \tag{14}$$

The normal stress in the fiber and the shear stress in the matrix are given by

$$\sigma_z^f=E_f[f'(z)+\eta\beta'(z)r\cos\theta],\quad 0\leqslant r\leqslant a \tag{15}$$

and

$$\tau_{rz}^m=-G_m\left\{\frac{f(z)}{\ln(b/a)}\left[\frac{1}{r}+\eta b\frac{1+a^2/r^2}{b^2-a^2}\cos\theta\right]+\eta\beta(z)\frac{a^2}{b^2-a^2}\left(1+\frac{b^2}{r^2}\right)\cos\theta\right\},\quad a\leqslant r\leqslant b. \tag{16}$$

Force equilibrium for the fiber in the z-direction reads

$$\int_0^a\int_0^{2\pi}\frac{\partial\sigma_z^f}{\partial z}r\,dr\,d\theta+\int_0^{2\pi}\tau_{rz}^m(a,\theta,z)a\,d\theta=0 \tag{17}$$

while the moment equilibrium of the fiber about the y-axis ($\theta=\pm(\pi/2)$) gives

$$\int_0^a\int_0^{2\pi}\frac{\partial\sigma_z^f}{\partial z}r^2\cos\theta\,dr\,d\theta+\int_0^{2\pi}\tau_{rz}^m(a,\theta,z)a^2\cos\theta\,d\theta=0. \tag{18}$$

Upon substitution of eqns (15) and (16) in expressions (17) and (18) we obtain the following field equations for $f(z)$ and $\beta(z)$:

$$f''(z) - \frac{k^2}{a^2} f(z) = 0, \quad k^2 = \frac{2G_m}{E_f \ln (b/a)} \tag{19}$$

and

$$\beta''(z) - \frac{l^2}{a^2} \beta(z) - \frac{n^2}{a^2} f(z) = 0 \tag{20}$$

where

$$l^2 = \frac{4G_m}{E_f} \frac{a^2 + b^2}{b^2 - a^2}, \quad n^2 = \frac{8G_m}{E_f} \frac{b}{(b^2 - a^2) \ln (b/a)}.$$

Note that eqn (19) is identical with the concentric result given in eqn (7). When higher order expansions in η are employed this is no longer the case and the field equations for $f(z)$ and $\beta(z)$ are fully coupled. The uncoupling in eqn (19) occurs because the lowest order correction to u_z^f is 0 (η^2).

For an extended medium and a semi-infinitely long broken fiber, $0 \leqslant z < \infty$, we have $f(z) = A e^{-k(z-a)}$ and the boundary condition at $z = 0$

$$\int_0^a \int_0^{2\pi} \sigma_z^f(r, 0, 0) r \, dr \, d\theta = -\pi a^2 \sigma_0$$

which, together with expression (15) gives $A = (\sigma_0/E_f)(a/k)$ whereby

$$f(z) = \frac{\sigma_0}{E_f} \frac{a}{k} e^{-k(z-a)} \tag{21}$$

as in eqn (8).

Since the disturbance introduced by fiber breakage involves no applied moment at $z = 0$, we have

$$\int_0^a \int_0^{2\pi} \sigma_z^f(r, 0, 0) r^2 \cos \theta \, dr \, d\theta = 0$$

whereby, in view of eqn (15), we obtain the boundary condition

$$\beta'(0) = 0. \tag{22}$$

Substituting (21) into (20), together with the condition (22) and the requirement that $\lim_{z \to \infty} \beta(z) = 0$ we obtain after several manipulations:

$$\beta(z) = \frac{n^2}{k^2 - l^2} \frac{\sigma_0}{E_f} \left[\frac{a}{k} e^{-k(z-a)} - \frac{a}{l} e^{-l(z-a)} \right]. \tag{23}$$

For realistic values of v_f $(0.4 < v_f < 0.7)$ k and l are of similar magnitude.

With $f(z)$ and $\beta(z)$ thus determined, eqns (10), (14)–(16), provide the "complete" solution to the perturbed field caused by the break of the inner fiber. The total field is given by adding $\sigma_z^f = \sigma_0$ to expression (15).

We are now in a position to assess the overload caused in the nearest neighboring fiber, centered at $r = h$, $\theta = 0$.

In contrast with the concentric case, when the overload caused by a fiber break is shared equally by all six neighboring fibers, we assume that in the eccentric case the burden is distributed proportionately to the six unequal angles subtended by the arcs which span

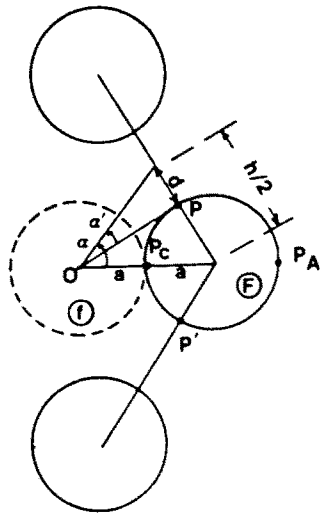

Fig. 5. Geometric considerations for evaluating the overload carried by the nearest neighboring fiber F due to the fracture of the fiber f. The load shed upon F is related to the angle α (see text).

the eccentric boundary relative to 0. Specifically, the angle α subtended by the nearest neighboring fiber F is shown in Fig. 5. A straightforward calculation gives $\alpha = \pi/12 + \alpha'$, where $\tan\alpha' = d/(\sqrt{3}a) = (h/2-a)/(\sqrt{3}a)$. Assuming that the overload $N(z)$ on fiber F is due to the shear stress $\tau_{rz}^{m}(b, z, \theta)$, $-\alpha \leqslant \theta \leqslant \alpha$, we have

$$N(z) = \int_{c}^{z} \int_{-\alpha}^{\alpha} \tau_{rz}^{m}(b, 0, z) b \, d\theta \, dz. \tag{24}$$

Substitution of eqns (16), (21) and (23) into expression (24) yields, after several manipulations

$$N(z) = \sigma_0 a^2 \left\{ \alpha e^{-k(z/a)} - \eta \sin\alpha \left[\left(\frac{b^2+a^2}{b^2-a^2} - \frac{8a^2b^2}{(b^2-a^2)c^2} \ln(b/a) \right) e^{-k(z/a)} + \frac{4a^2b^2}{(a^2+b^2)c^2} e^{-k(z/a)} \right] \right\}. \tag{25}$$

In (25) $c^2 = 2(a^2+b^2)\ln(b/a) - (b^2-a^2)$.

In addition to the normal overload, the shear stresses which act at the interface between the matrix and the nearest neighboring fiber introduce bending into that fiber. To assess the bending effect assume that these shear stresses are distributed uniformly over the arc PP' shown in Fig. 5. This would place the line of action of $N(z)$ at the center of gravity of the arc PP', hence with a lever arm $\rho = 3\sqrt{3}a/2\pi$ about the center of the nearest neighboring fiber.

Combining the normal and bending effects we have an overstress on the nearest neighbor

$$\sigma_{\substack{\max \\ \min}}(z) = \frac{N(z)}{\pi a^2}\left(1 \pm 4\frac{\rho}{a}\right) = \frac{N(z)}{\pi a^2}\left(1 \pm \frac{6\sqrt{3}}{\pi}\right). \tag{26}$$

Consider the corresponding non-dimensional quantity $\hat{S}(z)_{\substack{\max \\ \min}} = \sigma_{\substack{\max \\ \min}}(z)/\sigma_0$ then, employing superposition in analogy with eqn (9), the total non-dimensional stress in the fiber F is given by $S(z) = \hat{S}(z) + 1$ with $S(z)_{\max}$ occurring at point P_C and $S(z)_{\min}$ at P_A (Fig. 5).

3. RESULTS AND CONCLUDING REMARKS

The non-dimensional stresses $S(z)_{\substack{\max \\ \min}}$ borne by the fiber which is nearest to the broken filament are shown in Figs 6 and 7 vs the non-dimensional distance z/a from the place of the fiber break, for E-glass epoxy and graphite epoxy, respectively. For E-glass epoxy we took $V_f = 0.50$, $E_f = 10.5 \times 10^6$ psi and $G_m = 0.2 \times 10^6$ psi, while for graphite epoxy we employed $V_f = 0.65$, $E_f = 45 \times 10^6$ psi and $G_m = 0.2 \times 10^6$ psi.

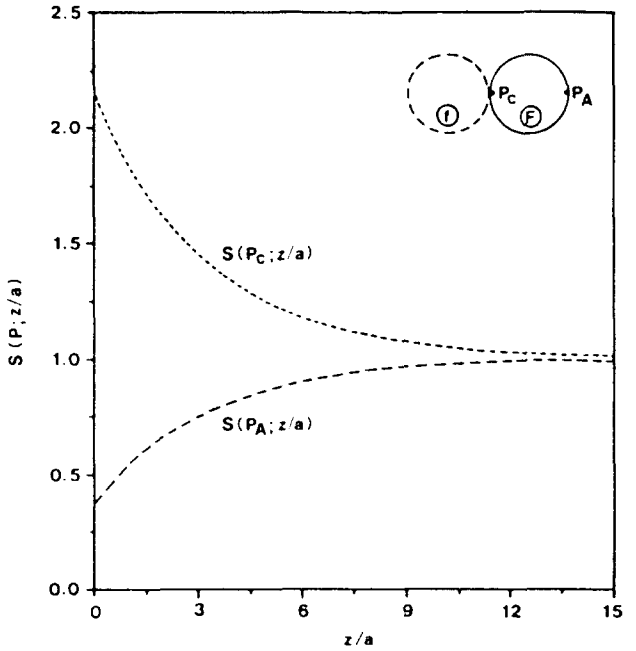

Fig. 6. The dimensionless stresses $S(z)$ carried by the fiber F at points P_C and P_A vs the non-dimensional distance z/a. Case of glass epoxy, with $V_f = 50\%$.

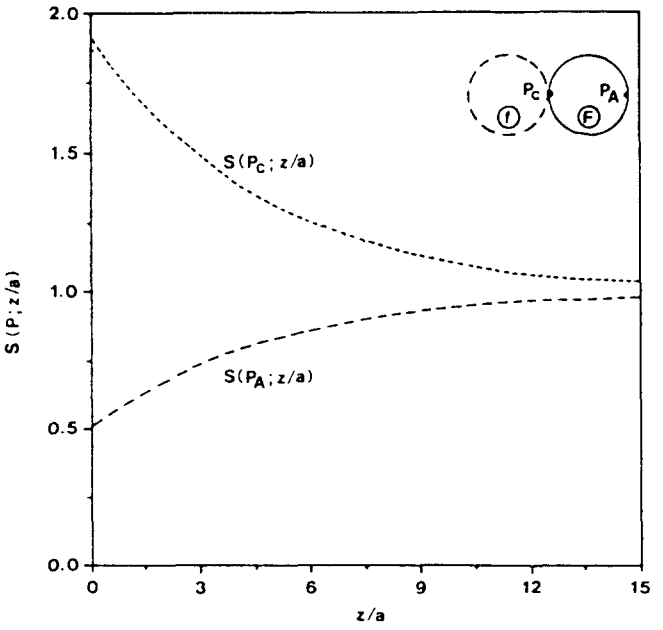

Fig. 7. Same as Fig. 6, but for the case of graphite epoxy and $V_f = 65\%$.

Note that a maximal stress increase of about 100% occurs in both glass epoxy and graphite/epoxy. This contrasts with rises of about 10–15% evaluated by Hedgepeth (1961). Furthermore, the effect of a fiber break is confined to a smaller distance in glass epoxy than in graphite/epoxy since the higher modulus of the graphite fibers introduces a stronger stress channelling effect due to the magnified anisotropy of the composite.

An account of the effects of overload on fibers near the broken filament was incorporated by Zweben and Rosen (1970), where all overloads were considered to be purely tensile and all fiber arrays were assumed to be periodic. They noted that fibers adjacent to the broken one would fail at the stress $\sigma_f K$, where σ_f is the nominal failure stress and K denotes the overload factor. Since fibers within composites are known to break even under low load levels the consideration of overload effects appears to be realistic. This argument applies in the present work as well, with the additional proposition that stresses due to fiber bending should be incorporated in the statistical analysis. Furthermore, it should be noted that due to the randomness of fiber spacing within the transverse cross-section the factor K should be viewed as a random variable and the statistical analysis should be reformulated to account for this fact. Finally, as indicated in the paragraph following eqn (9), normal stresses exist in the matrix (and fibers) in the transverse direction in the vicinity of a fiber break. A method to determine these stresses was developed, within the context of shear lag models, by Goree and co-workers [see e.g., Dharani *et al.* (1983)]. Obviously, such stresses would cause bending in neighboring fibers even in perfect arrays.

In view of the above considerations, it is clear that failure mechanisms quite distinct from tensile fracture can occur in fibers adjacent to a broken filament. Since it is reasonable to assume that imperfections of several kinds (such as weak, kinked, misaligned and broken fibers, debonds along fiber/matrix interfaces, voids and cracks within the matrix, etc.) are commonplace within fibrous composites, it is to be expected that the complex state of stress presented in this work should be routinely encountered in the vicinities of those imperfections. Consequently, the failure of filamentary composites may well be attributed to complex, mixed-mode mechanisms which are inherently different from those represented by the strength statistics of "dry" fiber bundles, which is associated with purely tensile response.

Acknowledgements—This research was supported, in part, by the Office of Naval Research under Contract N00014-90-J-1556, to one of the authors (YW). Dr Y. Rajapakse of the Mechanics Division, Engineering Sciences Directorate, has been the program manager.

REFERENCES

Christensen, R. M. (1979). *Mechanics of Composite Materials*. Wiley & Sons, New York.

Daniels, H. E. (1945). The statistical theory of the strength of bundles of threads. *Proc. R. Soc. (London), Series A*, **183**, 405–435.

Dharani, L. R., Jones, W. F. and Goree, J. G. (1983). Mathematical modeling of damage in unidirectional composites. *Engng Fract. Mech.* **17**(6), 553–573.

Garg, S. K., Svalbonas, V. and Gurtman, G. A. (1973). *Analysis of Structural Composite Materials*. Marcel Dekker, New York.

Gücer, D. E. and Gurland, J. (1962). Comparison of the statistics of two fracture modes. *J. Mech. Phys. Solids* **10**, 365–373.

Hedgepeth, J. M. (1961). Stress concentrations in filamentary structures. NASA Report TN D-882.

Hull, D. (1981). *An Introduction to Composite Materials*. Cambridge University Press, Cambridge, U.K.

McCarthy, J. M., Jr and Orringer, O. (1975). Some approaches to assessing failure probabilities of redundant structures. In *Composite Reliability, Sympos. Amer. Soc. for Testing and Materials*, pp. 5–28. ASTM, Philadelphia, PA.

Parnes, R. and Beltzer, A. I. (1986). Higher-order boundary perturbation method for asymmetric dynamic problems in solids—I. General formulation. *Int. J. Solids Structures* **22**(11), 1177–1187.

Prewo, K. M. (1986). Tension and flexural strength of silicon carbide fiber-reinforced glass ceramics. *J. Mater. Sci.* **21**, 3590–3600.

Rosen, B. W. (1965). Mechanics of composite strengthening. In *Fiber Composite Materials Am. Soc. of Metals*, pp. 37–75, New York. (Edited by S. H. Bush).

Schwietert, H. R. and Steif, P. S. (1990). A theory for the ultimate strength of a brittle-matrix composite. *J. Mech. Phys. Solids* **38**(3), 325–343.

Van Dyke, M. (1964). *Perturbation Methods in Fluid Mechanics*. Academic Press, New York.

Zweben, C. (1968). Tensile failure of fiber composites. *AIAA Jl* **6**, 2325–2331.

Zweben, C. and Rosen, B. W. (1970). A statistical theory of material strength with application to composite materials. *J. Mech. Phys. Solids*, **18**, 189–206.

APPENDIX: THE PERTURBATION EXPANSION

Consider two eccentric circles of radii a and b, respectively and with eccentricity e as shown in Fig. 4. As indicated in eqns (2) and (5), the solution to the concentric shear-lag problem is given by

$$u_z^f = u_z^f(z) = f(z) \tag{A1}$$

$$u_z^m = u_z^m(r, z) = \frac{\ln(b/r)}{\ln(b/a)} f(z) \tag{A2}$$

where according to eqn 8

$$f(z) = \frac{\sigma_0}{E_f} \frac{a}{k} e^{-k(z-a)} \quad \text{with} \quad k^2 = \frac{2G_m}{E_f \ln(b/a)}. \tag{A3}$$

In the eccentric case, considerations of static equilibrium for the fiber lead to the incorporation of a bending component in its deformation. Upon assuming that undeformed cross-sectional planes of the fiber remain plane after deformation, we choose in accordance with eqn (10):

$$u_z^f = u_z^f(r, \theta, z) = f(z) + \eta\beta(z) r \cos\theta \tag{A4}$$

where $\eta = e/b$. In the sequel, η serves as our perturbation parameter.†

In addition, by eqns (10)–(12), equilibrium of the matrix region yields

$$u_z^m = \frac{\ln(b/r)}{\ln(b/a)} f(z) + \left[\sum_{m=1}^{\infty} \left(A_m r^m + \frac{B_m}{r^m}\right) \cos m\theta\right] p(z). \tag{A5}$$

It is now necessary to satisfy the conditions that $u_z^m = u_z^f$ at $r = a$ and that $u_z^m = 0$ on the boundary of the *eccentric* circle of radius $r = b$.

According to the perturbation scheme of Parnes and Beltzer (1986) the value of a function $F(r, \theta)$ on the boundary C_0 of an eccentric circle of radius b with eccentricity $\eta = e/b$ can be expressed by a perturbation expansion in η as follows

$$F|_{C_0} = F^{(0)} + [F^{(1)} + {}_0\Phi_1^{(0)}]\eta + [F^{(2)} + {}_0\Phi_1^{(1)} + {}_0\Phi_2^{(0)}]\eta^2 + [F^{(3)} + {}_0\Phi_1^{(2)} + {}_0\Phi_2^{(1)} + {}_0\Phi_3^{(0)}]\eta^3 + \cdots \tag{A6}$$

where, in the present case

$${}_0\Phi_1^{(j)} = -b\cos\theta F_r^{(j)}, \quad {}_0\Phi_2^{(j)} = \frac{b}{2}[b\cos^2\theta F_{rr}^{(j)} - \sin^2\theta F_r^{(j)}] \quad \text{and}$$

$${}_0\Phi_3^{(j)} = \frac{b^2}{2}\cos\theta\left[\sin^2\theta F_{rr}^{(j)} - \frac{b}{3}\cos^2\theta F_{rrr}^{(j)}\right]. \tag{A7}$$

In the present problem the function $F^{(0)}$ is given in eqn (A4), and the boundary condition at $u_z^m/C_0 = 0$ is satisfied by the employment of expressions (A6) and (A7). On the other hand the continuity condition $u_z^m = u_z^f$ at $r = a$ does *not* involve the perturbation scheme since, by hypothesis, $r = a$ is a "concentric boundary". Obviously, the presence of two functions of z, $f(z)$ and $\beta(z)$, in eqn (A4) will necessitate two series expansions in (A5) (to assure $u_z^m = u_z^f$ at $r = a$). Denote the two series expansions by

$$\left[\sum_{m=1}^{\infty} \left(A_m r^m + \frac{B_m}{r^m}\right) \cos m\theta\right] f(z) \quad \text{and} \quad \left[\sum_{m=1}^{\infty} \left(\bar{A}_m r^m + \frac{\bar{B}_m}{r^m}\right) \cos m\theta\right] \beta(z), \text{ respectively.‡} \tag{A8}$$

Then, a systematic application of the conditions $u_z^m/C_0 = 0$ and $u_z^m(a, \theta, z) = u_z^f(a, \theta, z)$ yields

$$u_z^m(r, \theta, z) = \left\{\frac{\ln(b/r)}{\ln(b/a)} + \eta\left(A_1 r + \frac{B_1}{r}\right)\cos\theta + \eta^2\left[C_2 \ln(r/a) + \left(A_2 r^2 + \frac{B_2}{r^2}\right)\cos 2\theta\right]\right.$$
$$\left. + \eta^3\left[\left(C_1 r + \frac{D_1}{r}\right)\cos\theta + \left(A_3 r^3 + \frac{B_3}{r^3}\right)\cos 3\theta\right]\right\} f(z) + \left\{\eta \frac{a^2}{b^2 - a^2} \cdot \frac{b^2 - r^2}{r}\cos\theta\right.$$
$$\left. + \eta^2\left[\bar{K}_0 \ln(r/a) + \left(\bar{A}_2 r^2 + \frac{\bar{B}_2}{r^2}\right)\cos 2\theta\right] + \eta^3\left[\left(\bar{C}_1 r + \frac{\bar{D}_1}{r}\right)\cos\theta + \left(\bar{A}_3 r^3 + \frac{\bar{B}_3}{r^3}\right)\cos 3\theta\right]\right\} \beta(z) + O(\eta^4), \tag{A9}$$

where, upon denoting

† At first glance it may appear that the representation (A4) is somewhat arbitrary. However, it can be shown that if one starts with $u_z^f(z) = f(z) + \bar{\beta}(z) r\cos\theta$ then a systematic expansion in η indeed yields $\bar{\beta}(z) = \eta\beta(z)$. We chose (A4) as our starting expression to circumvent non-essential details.

‡ It is of course always permissible to include the "concentric" solution $A + B\ln r$ within the perturbation expansion whenever necessary.

$$A_0 = \frac{1}{\ln(b/a)}, \quad \bar{A} = \frac{a^2}{b^2-a^2},$$

we have

$$A_1 = -\frac{b}{b^2-a^2}A_0, \quad B_1 = \frac{a^2 b}{b^2-a^2}A_0, \quad A_2 = -\frac{1}{2}\frac{b^2}{(b^2-a^2)^2}A_0, \quad B_2 = \frac{1}{2}\frac{a^4b^2}{(b^2-a^2)^2}A_0,$$

$$C_2 = -\frac{b^2}{b^2-a^2}\frac{1}{\log(b/a)}A_0, \quad A_3 = -\frac{b^3}{3}\frac{1}{(b^2-a^2)^3}A_0, \quad B_3 = \frac{b^3a^6}{3(b^2-a^2)^3}A_0,$$

$$C_3 = -\frac{b}{b^2-a^2}\left[\frac{b^4}{(b^2-a^2)^2}+\frac{b^2}{b^2-a^2}\frac{1}{\log(b/a)}\right]A_0, \quad D_3 = \frac{a^2b}{b^2-a^2}\left[\frac{b^4}{(b^2-a^2)^2}+\frac{b^2}{b^2-a^2}\frac{1}{\log(b\ a)}\right]A_0,$$

and

$$\bar{K}_0 = -\frac{b\bar{A}}{\log(b/a)}, \quad \bar{A}_2 = -\frac{b^3\bar{A}}{b^4-a^4}, \quad \bar{B}_2 = \frac{a^4b^3\bar{A}}{b^4-a^4},$$

$$\bar{C}_1 = -\frac{b^2}{b^2-a^2}\left[1+\frac{1}{\log(b/a)}+\frac{b^4+a^4}{b^4-a^4}\right]\bar{A}, \quad \bar{D}_1 = \frac{a^2b^2}{b^2-a^2}\left[1+\frac{1}{\log(b/a)}+\frac{b^4+a^4}{b^4-a^4}\right]\bar{A},$$

$$\bar{A}_3 = -\frac{b^4}{b^6-a^6}\frac{b^4+a^4}{b^4-a^4}\bar{A}, \quad \bar{B}_3 = \frac{a^6b^4}{b^6-a^6}\frac{b^4+a^4}{b^4-a^4}\bar{A}.$$

The equilibrium of force and moment on the fiber, as given in equations (17) and (18), yield two coupled ordinary differential equations for $f(z)$ and $\beta(z)$. It turns out that $f(z)$ and $\beta(z)$ now take the following forms:

$$f(z) = \left(\frac{\sigma_0 a}{E_f k}+a_2\eta^2+a_1\eta^3\right)e^{-k(z/a)}+(\nu_2\eta^2+\nu_1\eta^3)e^{-l(z/a)}$$

$$\beta(z) = (\beta_1\eta+\beta_2\eta^2+\beta_3\eta^3)e^{-k(z/a)}+(\gamma_1\eta+\gamma_2\eta^2+\gamma_3\eta^3)e^{-l(z/a)} \tag{A10}$$

with

$$\bar{k} = k+\eta k_1+\eta^2 k_2+\eta^3 k_3, \quad \bar{l} = l+\eta l_1+\eta^2 l_2+\eta^3 l_3.$$

As noted earlier, we refrain from employing the higher order results of this Appendix in our computations, because the approximations involved in our model do not warrant their use. In fact, the utilization of higher expansions may convey the fallacious impression of higher accuracy.